THE DESIGN AND ANALYSIS OF A MAGNETIC WHEEL ENCODER FOR IMPROVING DISTANCE AND THROTTLE CONTROL OF AN AUTONOMOUS ALL-TERRAIN VEHICLE WITH AN INTERNAL COMBUSTION ENGINE

by

Joseph M. Phillips

A thesis submitted to the faculty of
The University of North Carolina at Charlotte
in partial fulfillment of the requirements
for the degree of Master of Science in
Electrical Engineering

Charlotte

2022

Approved by:

_____
Dr. James M. Conrad

_____
Dr. Valentina Cecchi

_____
Dr. Samuel Shue

ABSTRACT

JOSEPH M. PHILLIPS. Throttle Control Improvement of an Autonomous Vehicle with an Internal Combustion Engine. (Under the direction of Dr. James M. Conrad)

This work describes the integration of a rotary shaft encoder system through multiple layers of hardware and software abstraction for autonomous control of an All-Terrain Vehicle (ATV). The motor encoder info can be used in junction with the vehicle's kinematics to control its trajectory as it navigates its environment. The measurable data in question is related to velocity, distance travelled, and the angle of throttle movement. The encoder model was designed using computer aided design (CAD). The design utilizes a ring of evenly spaced magnets that is attached to the axle of the vehicle. The encoder spins the magnets trigger a Hall effect sensor that is attached to a 3-D printed mounting bracket bolted to the chassis. Each pulse represents a distance the vehicle has travelled and is added to a counter. Integration over time is used to measure the distance travelled within a second which can then be converted to velocity. The velocity and distance travelled is monitored using a micro-controller that sends instructions or commands to a servo controlled throttling system. The angular position of the servo is representative of a specific increasing or decreasing the throttle speed. An increase or decrease to the servos angle will slow down or speed up the vehicle. The encoders step resolution is 0.214 meters with eight pulses signifying a complete wheel rotation. The encoders highest trial error was 2 percent during a 550-meter test, and a 0.07 percent trial error during a 30-meter test.

ACKNOWLEDGEMENTS

I would like to take the time to acknowledge and thank every person that has guided me or helped me through this journey called life. Whether you have made an impact on my life in a negative or positive way, it has made me the person I am now, and I am greatful for that. I would especially like to thank my committee members Dr. Valentina Cecchi, Dr. Sam Shue, and my advisor Dr. James Conrad for their endless patience and guidance throughout my academic career. I am thankful for every oportunity they have given me to further my education.

TABLE OF CONTENTS

LIST OF TABLES

LIST OF FIGURES

LIST OF ABBREVIATIONS

AC	Alternating Current
AI	Artificial Intelligence
ATV	All-Terrain Vehicle
CAD	Computer Aided Design
CAN	Controller Area Network
DC	Direct Current
EPS	Electric Power Steering
IMU	Inertial Measurement Unit
ISR	Interrupt Service Routine
GPS	Global Positioning System
GPU	Graphic Processing Unit
GUI	Graphical User Interface
LED	Light Emitting Diode
ML	Machine Learning
MPH	Miles Per Hour
MPS	Meters Per Second
NI	National Instruments
OS	Operating System
PCB	Printed Circuit Board
PCM	Powertrain Control Module
PWM	Pulse Width Modulation
QRE	Quadrature Rotary Encoder

RC	Radio Controlled
ROS	Robot Operating System
RPM	Rotations Per Minute
SLAM	Simultaneous Localization and Mapping
V	Voltage/Volts
VS	Vehicle Speed

CHAPTER 1: INTRODUCTION

Today's society is moving quickly into artificial intelligence (AI) and autonomous vehicle technology. It is common for people to use multiple electronic devices throughout their day for assistance. Those devices, or small embedded computing systems can be used for mathematical computations, driving directions, or weekly scheduling. We are now using them to assist with driving vehicles. Vehicles come equipped with speed control, braking assist, and object detection. The advanced features of vehicles today can operate a vehicle autonomously and make the same high-level decisions expected of humans. Unlike larger computers, embedded computers installed within a vehicle are programmed with smaller operating systems that can process machine learning (ML), or AI neural networks. The decisions made by these embedded computers is only made possible from data provided by multiple sensors found within the vehicle. Examples of these systems would be brake-assist, cruise control, or object detection. If an object is detected a specific distance away when travelling a certain speed, a message is passed on to tell the vehicle to apply the brakes, autonomously slowing the vehicle down. Without vehicle sensors or systems, the vehicle could not make decisions autonomously. If an embedded system that is in control of a vehicle fails, it could lead to serious driving accidents or even death. Therefore, the investigation of control and automation of a vehicle must be evaluated thoroughly and must work with minimal error. This work will focus on an encoder device

that will more reliably send external data to an embedded device to improve the control architecture and facilitate precise control of a vehicle's dynamics.

1.1 MOTIVATION

The motivation for this work is the investigation and development of an autonomous vehicle. To implement and install higher levels of embedded computing such as machine learning with object detection or other machine learning networks a solid foundation of sensor data must be provided that has little error. This work will help with building a solid foundation for future work.

1.2 PROBLEM STATEMENT

The objective of this work is to provide accurate encoder sensor data that will be used in a control architecture of an autonomous vehicle. Embedded computing systems shall be able to use this data to facilitate acceleration, braking, and steering instructions to successfully operate an autonomous vehicle safely.

1.3 CONTRIBUTION

The contribution of this work describes the design of an encoder that can accurately communicate distance and velocity sensor data to other embedded computing systems of an autonomous vehicle. The encoder will allow the implementation of a new control architecture or framework that helps to integrate future sub-systems into a vehicle and is simple to debug if necessary.

1.4 REMAINING AND FUTURE WORK

Remaining work for this study is to decrease the error of the added encoder sensor. This could be done using sensor fusion along with an inertial measurement unit (IMU). The ATV would need to be equipped with a reliable breaking and steering system. The previous working systems could be updated provided the hardware is compatible with new working technologies. Once the four core data feedback systems are in place (encoder, throttle, breaking, steering), machine learning with object detection, simultaneous localization, and mapping (SLAM), and other algorithms could be applied using a dependable graphic processing unit (GPU) along with multiple embedded system controllers. The vehicle is planned to be ROS-enabled with sufficient simulation and model testing. Robot Operating System (ROS) will provide an easier way to initially evaluate movement algorithms, saving time with less risk of damaging the vehicle during physical testing.

CHAPTER 2: THEORY AND BACKGROUND

2.1 ATV SPECIFICATIONS AND BACKGROUND

The following list represents the key features and aspects of the ATV.

- Make: Honda
- Model: Rancher TRX420FPE
- Year: 2009
- Engine: 420cc single-cylinder four-stroke
- Drivetrain: Electric Shift (Gear Levels 1-5 and Reverse)
- Drivetrain: 2-wheel and 4-wheel drive
- Electric Power Steering (EPS)
- Multifunctional Display
    - Speed (MPH)
    - Mileage
    - Transmission positioning
    - Engine or PCM errors

FIGURE 2.1: Honda ATV 2009 420 Rancher.

2.2 PREVIOUS PROJECTS AND WORK

This ATV was a part of several efforts to implement control architecture for automation. In 2010, methods to steer and control the ATV were investigated. This work investigated ways to control the ATV autonomously [1]. A Renesas and RS-232 microcontroller was used to digital control the sub-systems and a LIDAR was installed for object detection. A linear actuator was installed to help apply the brakes and a servo was used installed to control the throttle. The system was based off a rotary encoder that was installed on the existing electric power steering (EPS) and detected the steering angle of the ATV. Complications arose when the EPS system kept overheating due to the large current draw of the EPS motor.

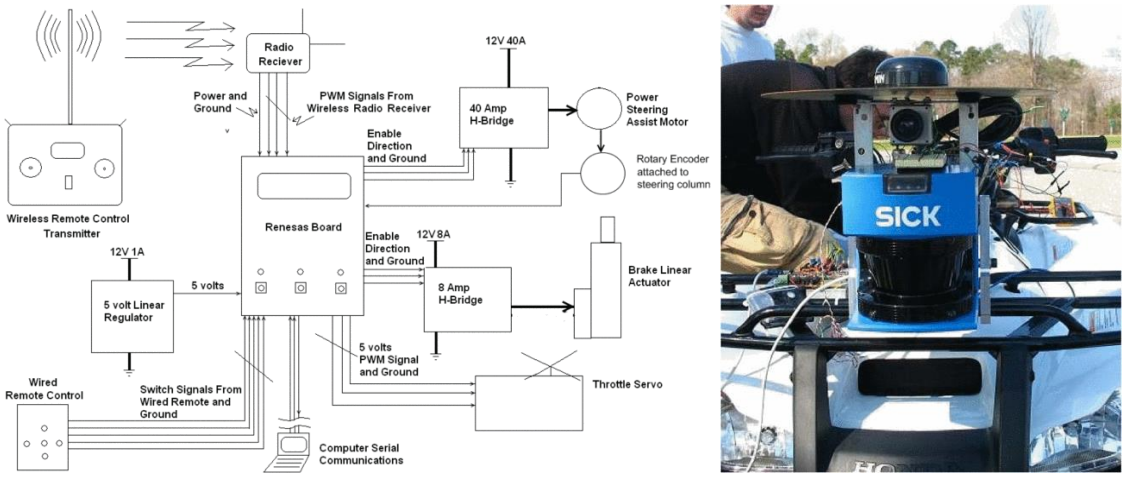

FIGURE 2.2: Previous electrical design and LIDAR system. [1]

In 2012 more work assessed the overheating problem with the control of the steering [2]. Hardware and software techniques were utilized to solve the problem. A new state machine was implemented with newer microcontrollers and a power conditioning circuit was designed. An open and a closed loop circuit were evaluated and compared to address steering issues. An open-loop system with no feedback reduced the heating of the EPS motor, but induced error into the navigation system. A closed-loop system with feedback control had impressive results in testing, but the EPS motor had significant warming. This suggested that the motor may need to be replaced with a larger one or one would need to use an open-loop system and somehow make up for the steering error.

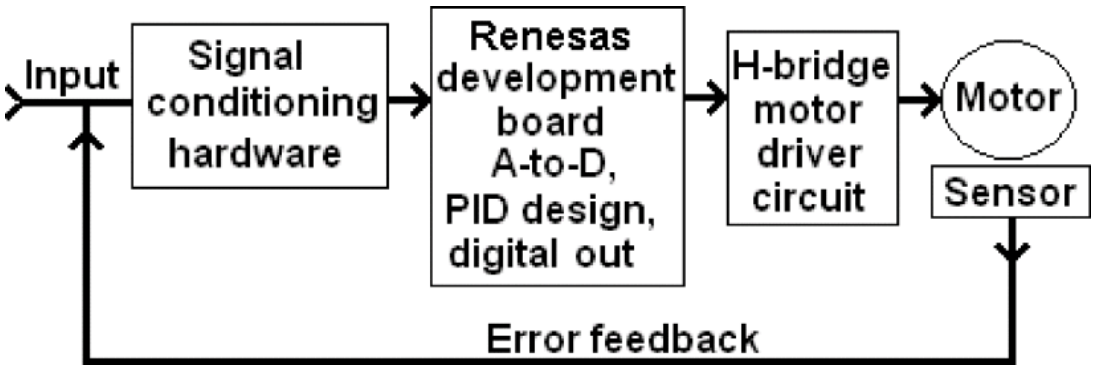

FIGURE 2.3: Closed-loop digital control system [2].

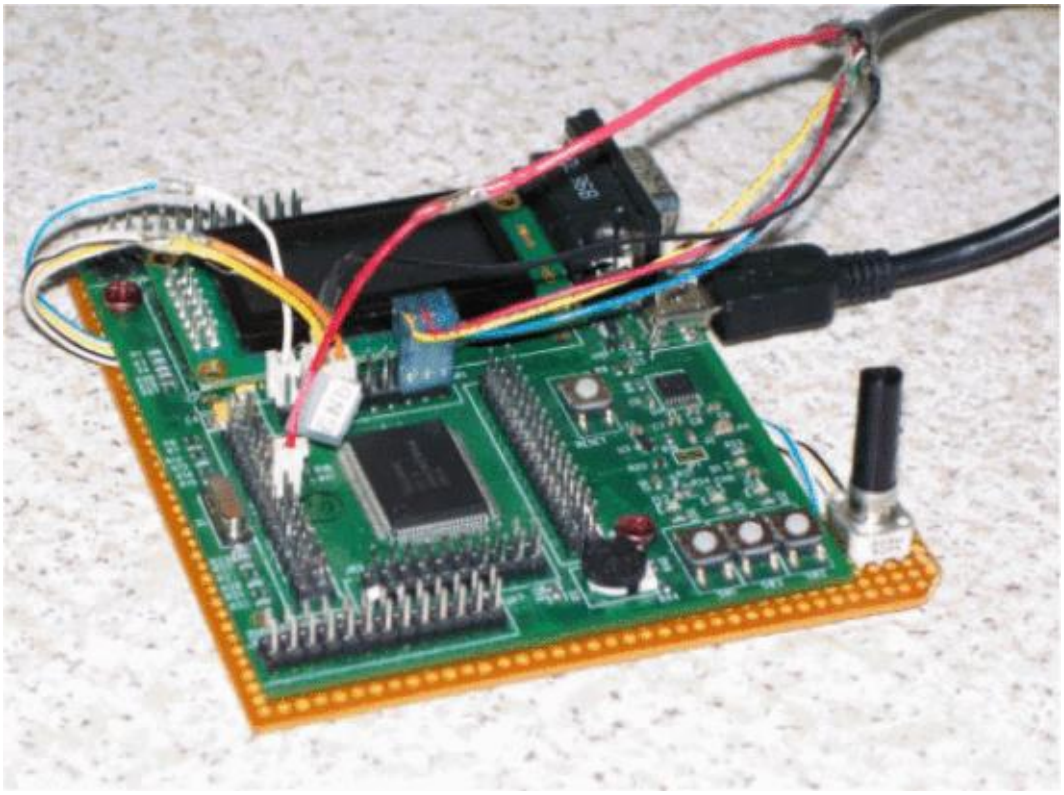

FIGURE 2.4: Renesas microcontroller input [2].

Later in 2014, a Controller Area Network (CAN bus) system was designed for the ATV [3]. This work investigated signal noise reduction and to replace obsolete or broken peripherals. This new CAN bus system would also control the steering, throttle, and brakes using a Renesas RX63N as the brain and CAN modules and transceivers. The braking system was replaced by a different and better power efficient motor controller. A new CMOS analog switch was added to the EPS system and utilized in a closed-loop feedback system. This new steering system was an improvement over previous designs, but over heating still occurred if the ATV was sitting still while changing the steering angle due to the friction of the tires on the ground. The ATV was fully operational using a radio controlled (RC) transmitter to control the throttle, braking, and steering systems.

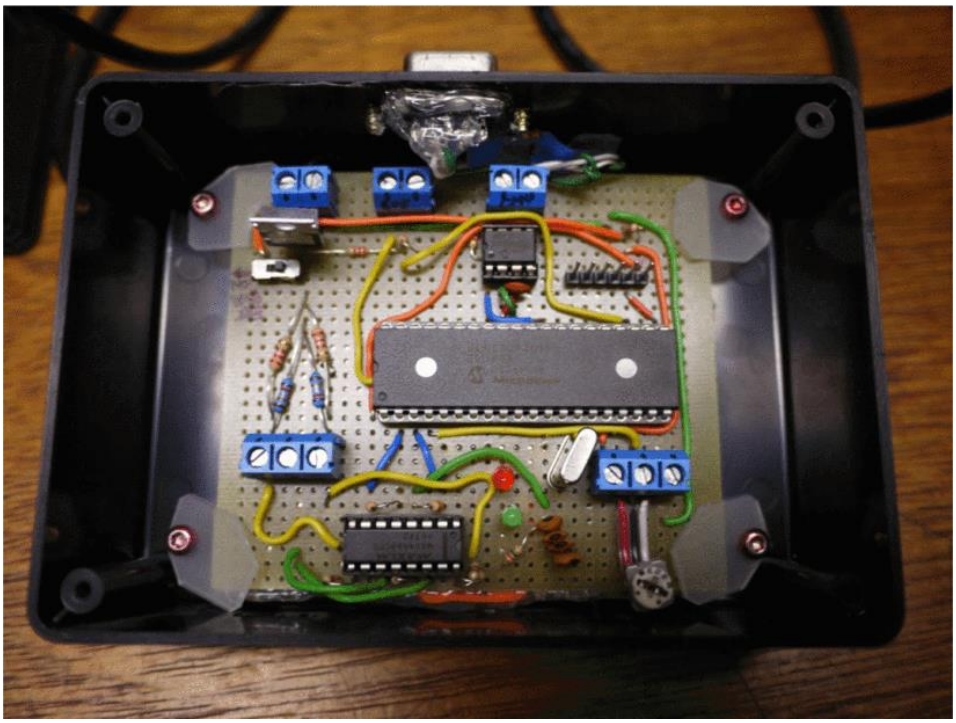

FIGURE 2.5: New steering control node installed [3].

The ATV was used in 2018 for a paper and research into topology classification for autonomous vehicles using its existing CAN bus system for messaging [4]. This assessed the problem of learning how to navigate through areas by identifying objects, classifying them, and determining how to navigate through the classified area with global positioning system (GPS). A wireless network sensor was used to classify objects and relay the data. This proposed method would be used to make the ATV a semi-autonomous vehicle.

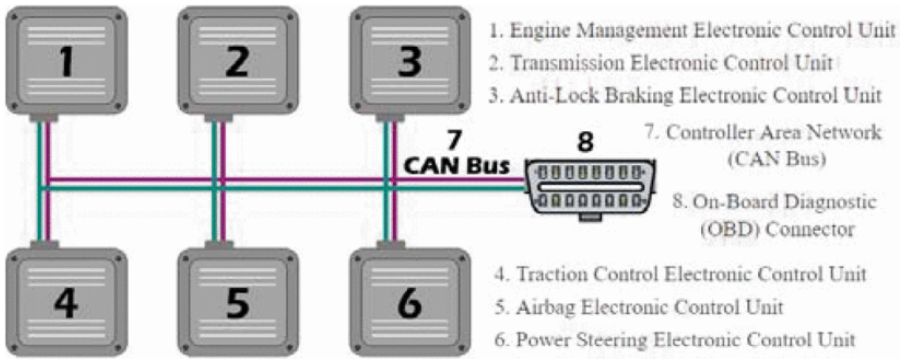

FIGURE 2.6: Example CAN bus diagram [4].

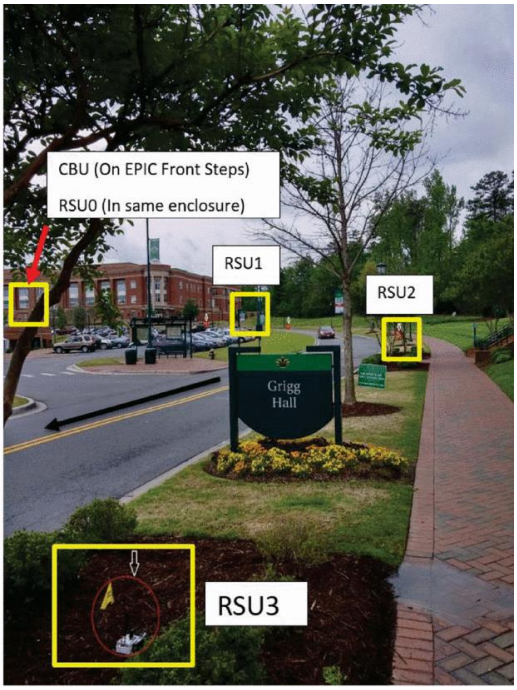

FIGURE 2.7: Road-side units deployed on campus [4].

In the same year, other work describes how the ATV was ROS-enabled to simulate sensors and other robotic functions by converting the existing systems into ROS based platforms [5]. This system was designed to utilize National Instruments (NI) hardware with the accompanied LabVIEW software. A myRIO controller was used to fully take advantage of the ROS toolkits developed for LabVIEW. This allowed the use of a pre-made ROS framework that could publish and receive messages without creating one from scratch. After ROS integration, an attempt at providing velocity feedback was investigated, and a quadrature rotary encoder (QRE) was developed. This QRE was specifically designed to provide feedback to ROS regarding the ATV's speed of travel. This was the first effort towards abstraction of the ATV's velocity or speed into a computing system. This work successfully integrated the ATV in ROS which aids in the continuing objective to make the ATV fully autonomous.

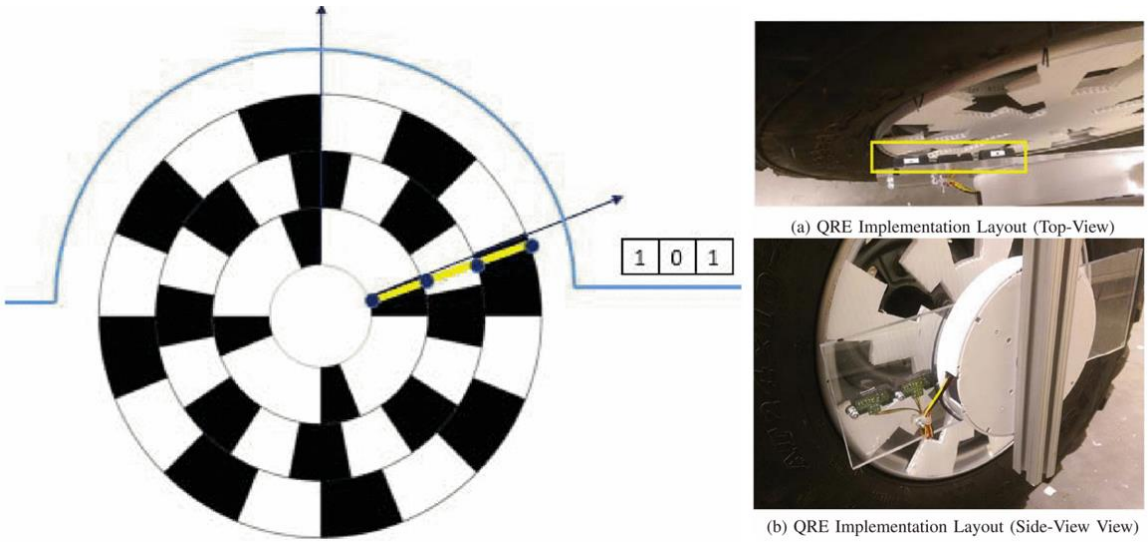

FIGURE 2.8: QRE implemented for speed readings [5].

The CAN bus system was later modified in 2019 to work with Texas Instrument's MSP430 microcontrollers [6]. The braking, steering, and throttle systems were all updated with MSP430 microcontrollers, and custom CAN bus printed circuit boards (PCB) were designed for integration and communication with the MSP430. A GPS in conjunction with a IMU were also integrated into the system to detect the position and orientation of the ATV as it travelled. This system was also used as an attempt to abstract the velocity or speed of the ATV as it travelled, but its viability was limited due to the latency and real-time reaction of the GPS unit. Speed or velocity abstraction was attempted due to the previous QRE system. The QRE system was evaluated in a controlled environment, and it was later found that evaluating it in the field yielded unreliable data due to mechanical and environmental variables. The QRE operation was hindered by path debris that caused damage. The ATV would encounter uneven terrain in path environments causing negative and positive forces on the ATV's suspension. The QRE sensor is not static to the ATV and

the vertical forces induced error in the sensor readings. The designed wheel hub encoder was easily damaged on uneven terrain and incurred damage over time hindering the output data as well.

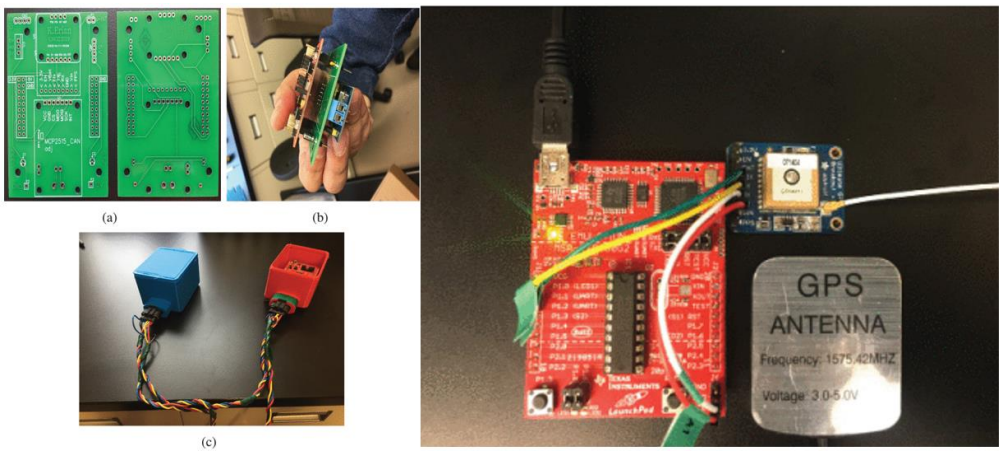

FIGURE 2.9: MSP430 and GPS with CAN bus design [6]

As mentioned before, the second attempt of abstracting the ATV's speed data was limited due to latency involved with a GPS system. As an alternative, in 2021 work was done to investigatee ATV's internal speed control circuit [7]. The ATV itself has a multi-functional display that reports the speed in miles per hour (MPH) to the rider. This prompted an investigation as to how the ATV reports this data. The ATV has two vehicle speed (VS) sensors. The rear VS sensor in the circuit is the main sensor that is located directly on the engine. This VS sensor feeds data back to the powertrain control module (PCM) and other junction modules. The second sensor is located in the front drivetrain of the ATV. The ATV can be operated in 2-wheel and 4-wheel drive mode, and the front VS sensor is only effective when the ATV is in 4-wheel drive. When assessing the VS sensor signal with an oscilloscope, it was discovered that when the vehicle is in 4-wheel drive, they produce the same digital pulse data. The readings where originally taken directly from the sensor itself, but this proved unreliable due to the noise and vibration produced by the

ATV when running. Successful readings were taken at the junction modules where the sensor data is distributed to the EPS, and PCM systems. Code was written for the MSP430 to trigger when a pulse is detected from the rear VS sensor and then converted to a speed (MPH) threshold that could naturally be understood by anyone. This method proved dependable and successful for speed control in all ATV conditions and environments travelled. The second modification came to the steering system that was previously in place. Due to the EPS motor over heating related to wheel and ground friction, a new steering method was installed that provided sufficient torque utilizing less power. This steering method included adding a new similar motor as the EPS system to the back of the ATV with a pully system. The motor was driven by an external motor driver and was controlled by pulse width modulation (PWM) signals from an MSP430. Stainless steel wire rope cable is attached to both handlebars simulating how a real person would steer the ATV. This device needed to produce 50-lbs of force to turn the steering column and did so successfully with ease. While it is not an ideal look, this solved the steering issues for the ATV. The ATV was able to drive at a controlled speed while accepting steering commands at the full Honda manufactured range.

FIGURE 2.10: Engine VS Sensor wire [7]

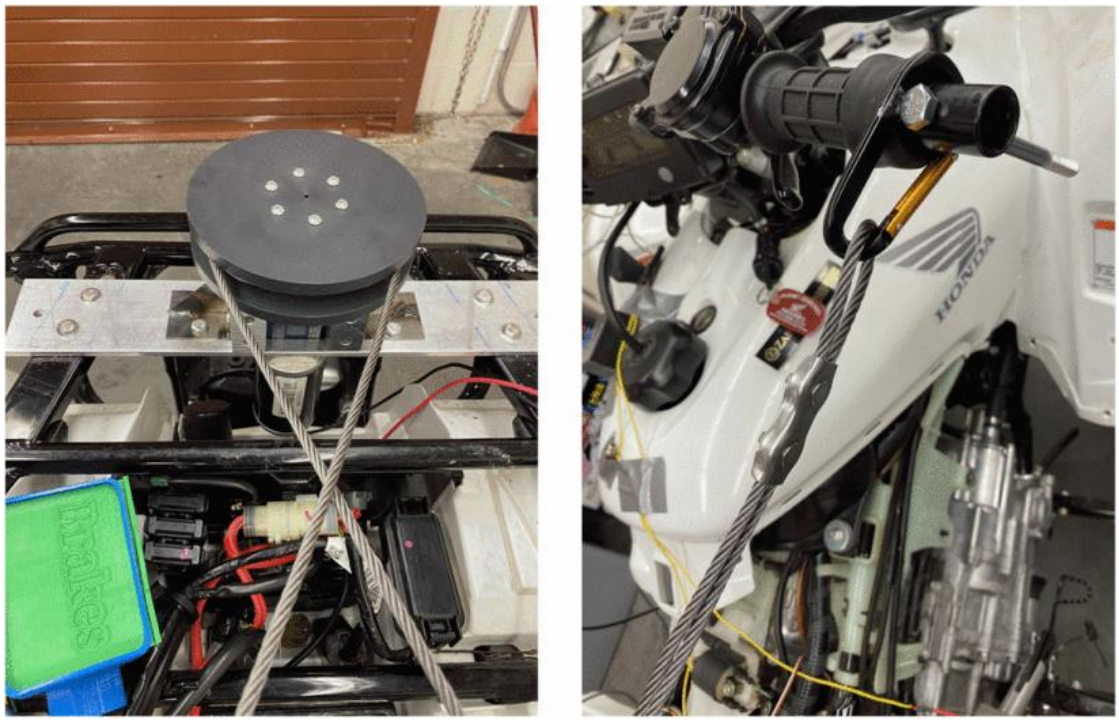

FIGURE 2.11: New motor driven handlebar steering system [7]

In 2021, work was started to move forward with plans to make the ATV fully autonomous [8]. The throttle, and steering systems could now be controlled with AI using machine learning algorithms. This was implemented by adding a Nvidia Jetson Nano 4Gb GPU to the ATV. The original core systems were still controlled by MSP430's. The GPU used a camera system to compare live data to a trained segmentation machine learning model to predict steering angles to keep itself on a pathed pathway. The speed control was kept at a consistent operational value for safety. The ATV makes slight steering angle adjustments when it determines it close to running off the path. This work proved successful as the ATV was able to follow the path autonomously making steering adjustments on its own. for a good amount of time. Some issues and concerns were encountered when there was not enough light on the pathway making it hard for the machine learning model to make the correct steering predictions.

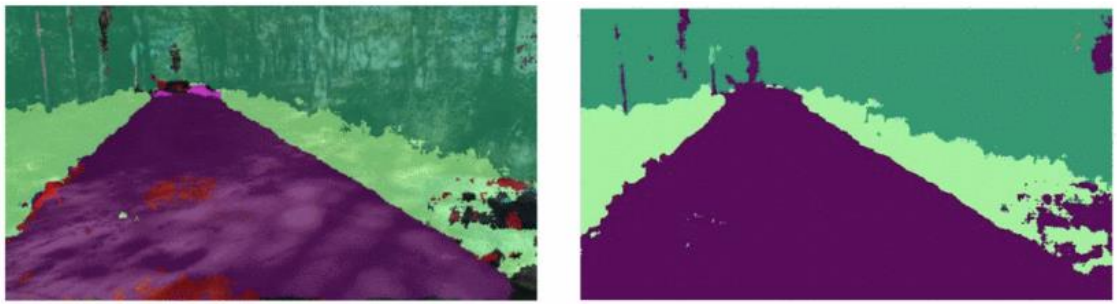

FIGURE 2.12: Neural network segmentation output [8]

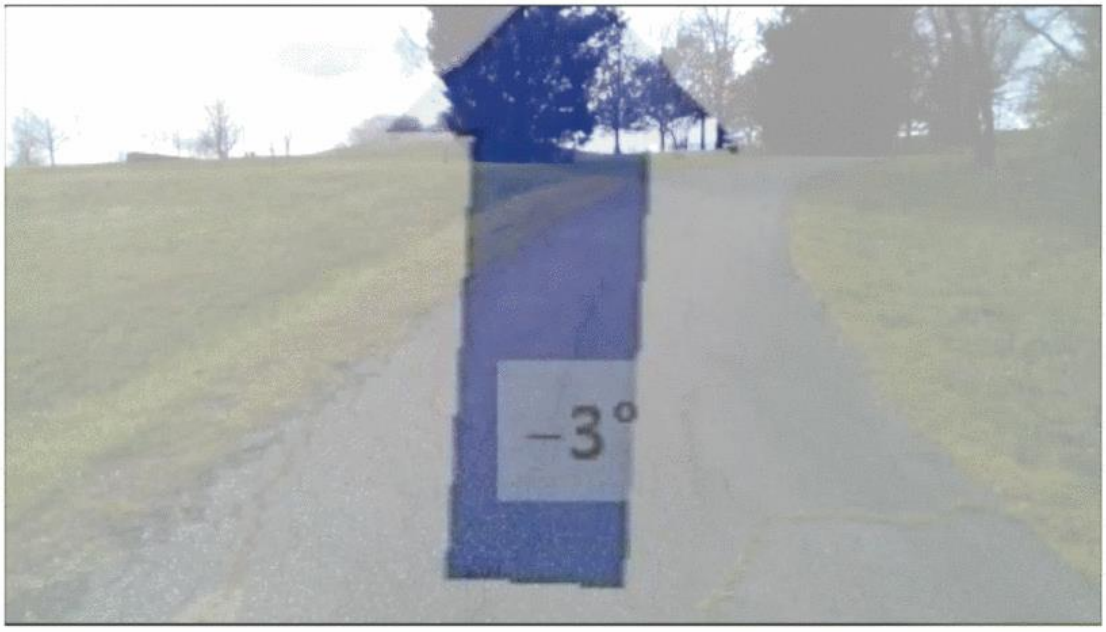

FIGURE 2.13: Steering angle visualization and feedback angle [8]

2.3 ENCODERS

Encoders are mechanisms or devices that enable one to retrieve data feedback about the motion of an object. There are several types of encoders such as linear, rotary, angle, absolute, and incremental. They are usually implemented into control systems. The data retrieved by the encoder can be used to control a single object or many objects within a system such as a motor. An example of this would be monitoring the shaft of a motor

which could indicate the rotations per minute (RPM) or velocity of the motor. Encoders use different technologies for sensing such as capacitive, optical, and magnetic.

2.3.1 OPTICAL ENCODERS

Optical encoders are the most accurate of encoder sensors depending on the operating environment. They use a light source such as an infrared LED, visible LEDs, miniature lightbulbs, or laser diodes that are converted to an electrical signal depending on the reflection sent back. The sinusoidal signal is then converted to a digital high or low pulse making up a square wave. Each pulse is counted and referenced to a linear or angular position which changes over time. Knowing this allows one to track the motion of an object.

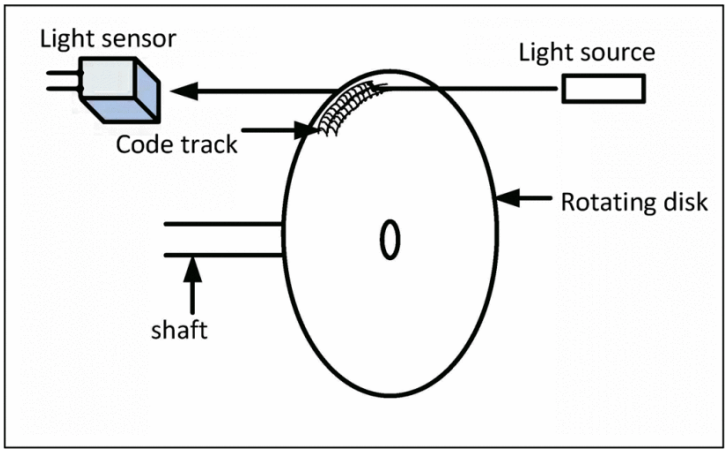

FIGURE 2.14: Optical encoder diagram [9]

2.3.2 CAPACITIVE ENCODERS

Capacitive encoders rely on the change in capacitance or repeated distortion in an alternating current (AC) field. The encoder is made up of three parts: a rotor, stationary receiver, and a stationary transmitter. The electrical signal is generated by the transmitter

which passes through a rotor, and the receiver converts the electrical signal to a digital high or low pulse. These pulses are counted and can be translated to the motion of an object.

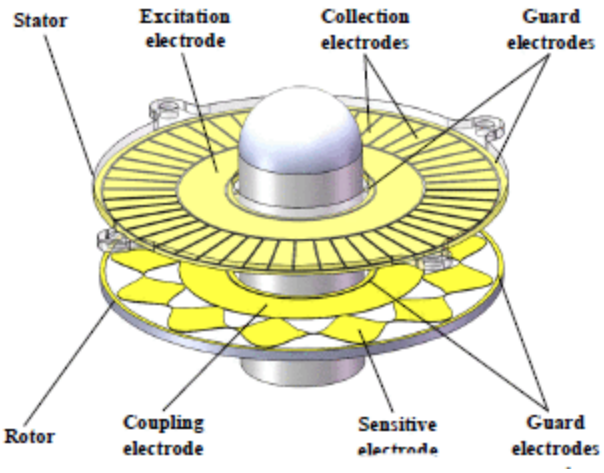

FIGURE 2.15: Structure of capacitive rotary encoder [10]

2.3.3 MAGNETIC ENCODERS

Magnetic encoders consist of multiple magnetics with a specific number of poles. They are commonly used as rotary encoders where the magnets are positioned around the circumference of the encoder. The encoder can have multiple channels. Having multiple channels allows the tracking of direction. A Hall effect sensor is used in conjunction with the rotary encoder and detects the change in voltage or magnetic flux to determine movement. The change in the magnetic field creates a sinusoidal electrical signal that is then converted to a digital high or low pulse. These pulses are used to count rotations that are translated into linear or angular movement.

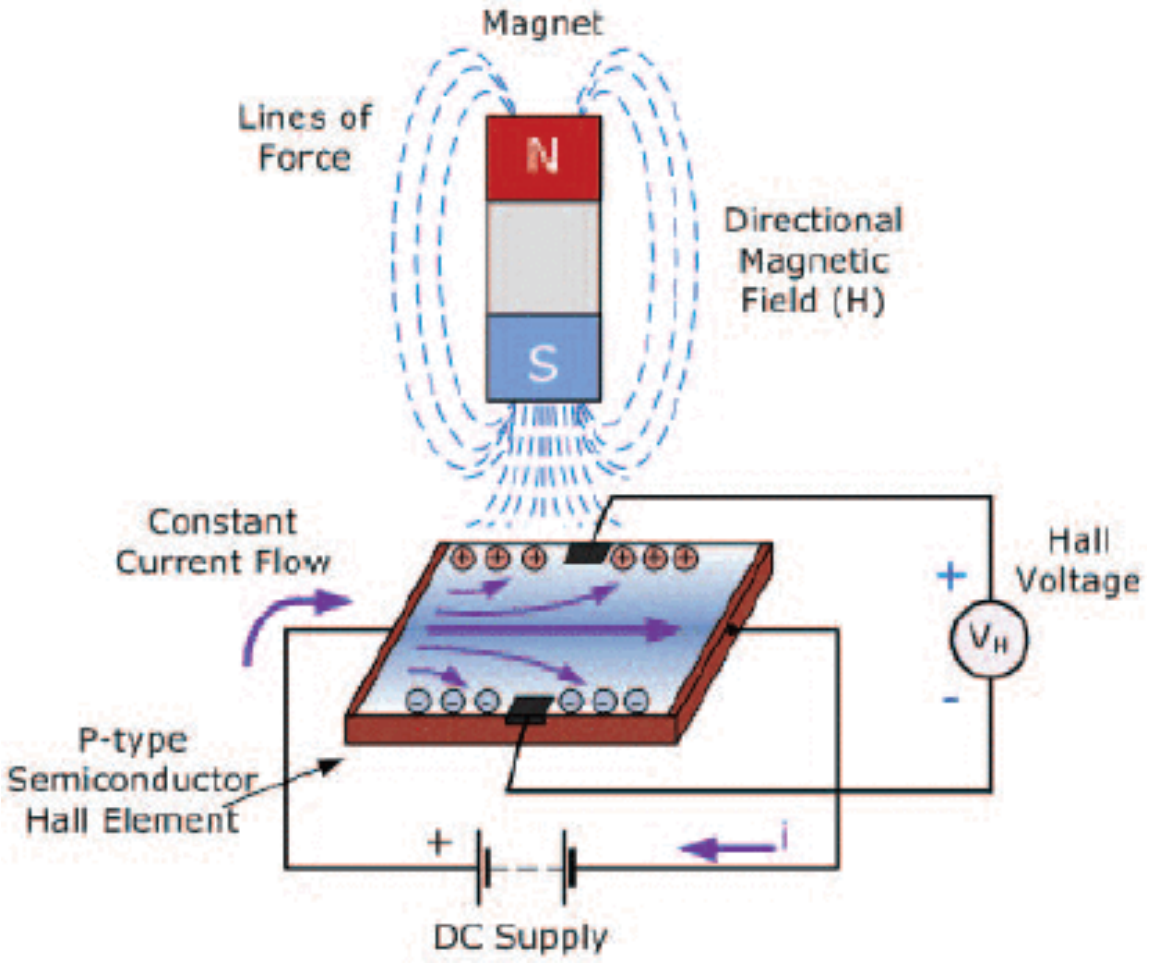

FIGURE 2.16: Magnetic field detected by the Hall effect sensor [11]

When choosing the type of encoder to use for a specific application, there are several categories to consider. Environmental factors play a significant role in deciding the type of encoder application. External light, or dust in the air can induce error into an optical encoder system. External electrical fields can induce error into a capacitive or magnetic encoder system. Wire shielding may be needed to prevent external influences such as vibrations from inducing error. Some of the categories for review can be seen in the table below.

TABLE 2.1: Factors to consider for encoder types

<table>
<tr><th colspan="5">Encoder Factors to Consider</th></tr>
<tr><th>Measurement</th><th>Motion Involved</th><th>Environment</th><th>Electrical</th><th>Mechanical</th></tr>
<tr><td>Position</td><td>Linear</td><td>Temperature</td><td>External Field Influences</td><td>Shaft or Linear</td></tr>
<tr><td>Angle</td><td>Rotational</td><td>Dust/Moisture</td><td>Power Consumption</td><td>Rotary</td></tr>
<tr><td>Velocity</td><td rowspan="2">Directional</td><td>Vibration</td><td rowspan="2">Wire or Interface Shielding</td><td rowspan="2">Mounting Area</td></tr>
<tr><td>Resolution</td><td>External Light</td></tr>
</table>

2.4 HALL EFFECT SENSOR

Hall effect sensors can detect the Hall Effect. The Hall Effect, discovered in 1879 by Edwin Hall, occurs when a magnetic field comes close enough to a conductor causing the change in potential difference. This change in potential is usually caused by the magnitude of a magnetic field. The force exerted on the conductor is known as the Lorentz Force [12].

The Lorentz Force can be expressed and seen below using the electric (E) and magnetic (B) fields applied to a charge (q) and its velocity (v),

$$F = q(E + v \times B) \tag{1}$$

where x is the cross product and E, B, v are vectors.

This can also be expressed directly in terms of scalar and vector potential, taken from the charge and current density,

$$F = q\left(-\nabla\Phi - \frac{\partial A}{\partial t} + v \times \nabla \times A\right) \tag{2}$$

where Φ is the electric scalar potential and A is the magnetic vector potential.

This allows one to measure the magnitude of the magnetic field, or simply switch a circuit on or off. Hall effect sensors are commonly used in automotive systems for position sensing applications. They would be used to measure the speed of a shaft for tachometers, braking systems, or ignition timing. To accomplish this measurement, a Hall effect sensor would be used in conjunction with a rotary shaft encoder that includes some type of magnetic field generator. As the magnetic field passes over the Hall effect sensor, an electric signal is generated and then converted to a digital high or low pulse that a system is designed to read.

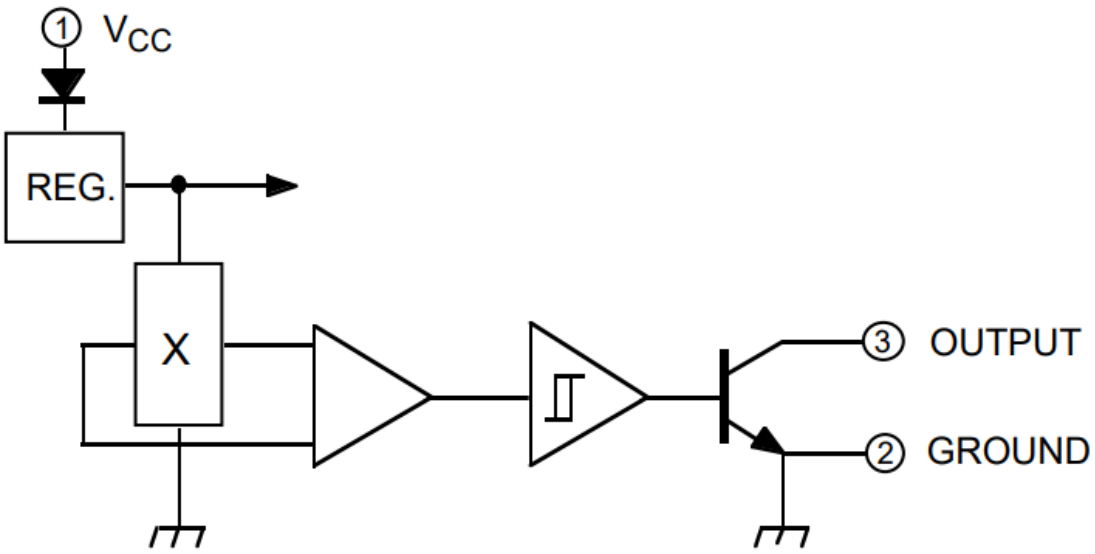

FIGURE 2.17: A3144 Hall effect sensor circuit diagram [13]

2.5 ROS

ROS helps to build robot applications using state-of-the-art algorithms and developer tools. ROS is technically not an operating system (OS) but is middleware that allows the integration of external robotic hardware platforms. The user can breakdown their robot components into nodes and these nodes can send or receive data messages about their

location or position. ROS also has built in software to monitor and simulate robotic applications using a graphical user interface (GUI) such as RVIZ or Gazebo [14]. Gazebo simulates a 3D indoor or outdoor environment that users can evaluate their robot or robot sensors effectively. These applications allow users to visually assess and analyze how the robot applications will perform before live testing. These applications are useful because designers can evaluate and achieve a desired output to ensure their robotic design works before physically testing it. A robotic vehicle could be evaluated in a virtual environment to ensure turning, braking, and velocity commands are being interpreted and simulated correctly. The ROS simulations are time and cost effective and limit the risk of robot damage from live testing.

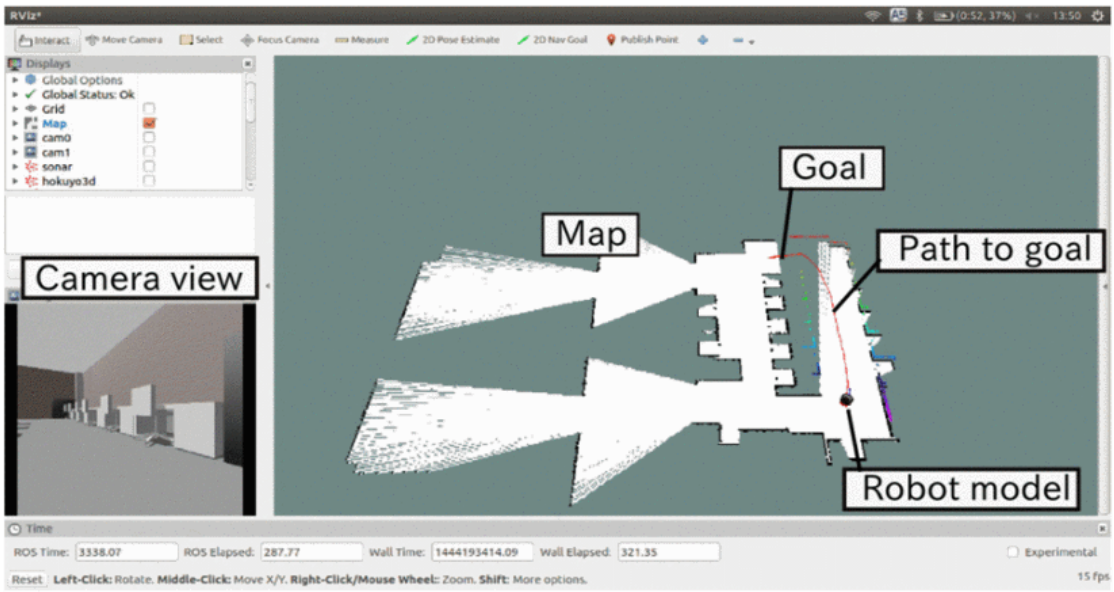

FIGURE 2.18: ROS robotic path planning simulation example [14]

CHAPTER 3: ATV TROUBLESHOOTING

3.1 SEARCHING FOR A SIGNAL

Our Honda ATV is equipped with a multifunction digital display. It shows the speed, current accumulated mileage, engine hours, gear position, and oil change indication. Since the ATV is already using a signal to translate and display the speed on the display, this same signal could be used to interpret and communicate a speed to external sources such as a microcontroller. The ATV is equipped with two VS sensors. The sensors were investigated with an oscilloscope to check the data being sent. The rear VS sensor is mounted directly on the motor and this signal proved to be very noisy and was not useful. The other two sensors provided clean digital pulses that could be read. With the ATV at idle, the system produced were fifteen per second. As the throttle was increased the pulses increased. By referencing the display speed on the multifunction display and increasing the throttle, a scale for speed could be created as compared to how many pulses were being read. This method was used in a previous project and proved useful but was only accurate when travel was for a consistent speed in the same gear position. Changing gears would change the number of pulses per the speed scale created. The speed scale was no longer valid, and the speed determined was incorrect. The pulses received from the VS sensor also had no relation to the distance being travelled by the ATV. There was no way to tell what these pulses meant and were a random speed signal abstraction. This method was abandoned for the following project and a new method was introduced. Instead of using an

internal signal from the ATV itself, it was decided to produce an external signal by designing and installing an external foreign sensor to detect the distance travelled by the ATV, and its current speed.

3.2 VIBRATION AND NOISE

As mentioned before, the ATV is very loud and produces a lot of vibration due to the internal combustion engine. This can lead to unwanted noise in the electrical system. In previous projects electrical interference was experienced and a CAN bus messaging system was installed which can eliminate electrical noise in signals, but this system has since been removed. The ATV itself does not use CAN bus from the factory, and after further investigation it was determined the CAN bus system is not absolutely needed. The original signal going into the CAN bus system is already distorted, and the CAN bus system does not function as a filter. CAN bus is just a digital communication protocol for transferring signals. Therefore, it was beneficial to find a more reliable analog speed signal elsewhere on the ATV to read from. Since there are mechanical and electrical properties of the ATV that cause electrical interference, this needs to be avoided by relocating sensor or computer wiring to a different location. The wiring should be as short as possible and shielded from any electrical interference that may occur. This is a common electrical practice in all vehicle applications. As seen in Figure 3.1, an extra fuse box and accessory power outlet were added to keep wire management organized. These two devices will enable wires to be kept short for powering extra peripherals on the ATV keeping the risk of noise or interference small. In Figure 3.2, one can see the wood platforms installed on the ATV's utility racks. These will shield debris and other objects from encountering other peripherals or electrical and mechanical components.

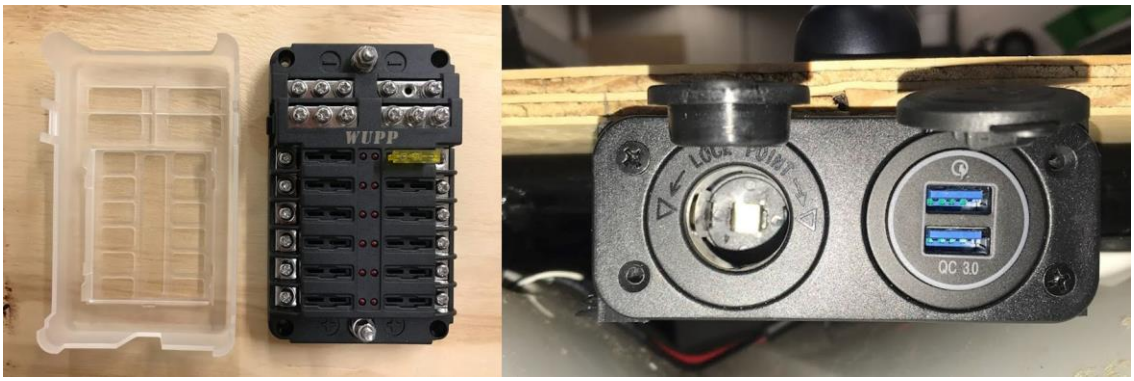

FIGURE 3.1: Fuse box and ACC outlet addition

FIGURE 3.2: Installed platforms to utility racks

Due to the vibration and noise from the internal combustion engine, the electrical interference can be large or small depending on the size and RPMs of the engine. An accelerometer was used to measure the vibration in the X, Y, and Z directions. As the throttle is increased, the RPM's rise, and the vibration and noise increase. This is common

with combustion engines and is an expected problem that must be overcome with the solutions mentioned above and seen below.

3.3 SENSOR LOCATION AND PLACEMENT

To design an external foreign sensor there were many factors to consider. One of the more key factors was placement or mounting location. To adapt a sensor to the mechanics of the ATV, a factory location that already had bolts or fasteners in place could double as a location to attach a sensor. The placement of the sensor determined its entire design, so this was important not have any mechanical design flaws going forward. The ATV had a lot of open space on the rear of the vehicle by the braking and drivetrain system that was an ideal place for sensor installation on the rear axle of the vehicle to measure wheel rotations. The drivetrain included mounting brackets and plates that served as physical protection from debris during travel. The existing plate fasteners or bolts could be used to hold the sensor in place if needed. It was important to make sure that loosening any bolts or fasteners on the ATV would not compromise the factory design or hinder how it operates in anyway. The brackets in question did not serve any mechanical functionality to the ATV so it was acceptable to use the existing bolts to attach the sensor for installation.

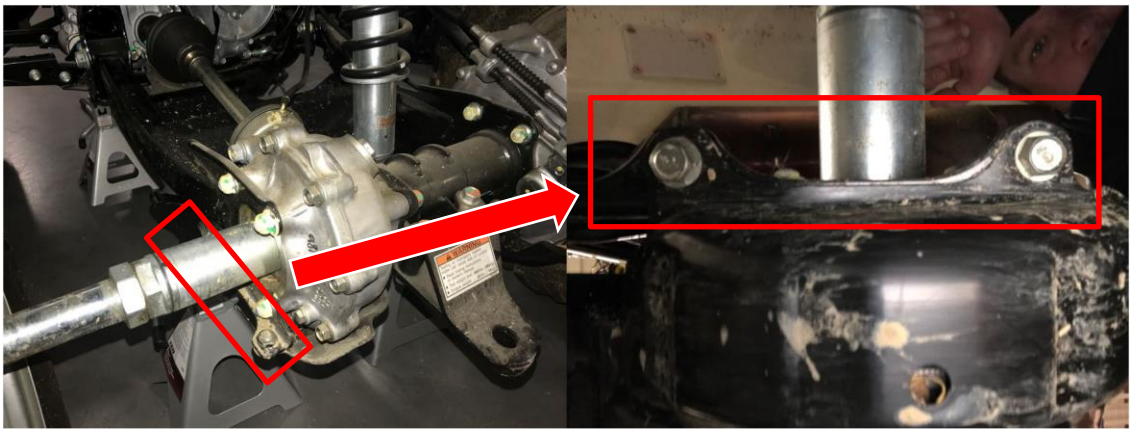

FIGURE 3.3: Rear axle and bracket assembly of the ATV

CHAPTER 4: ENCODER DESIGN, TESTING, AND RESULTS

4.1 SENSOR BRACKET DESIGN

The Hall effect sensor selected had a small design, so the bracket design to attach it could be small and lightweight. It was determined that 3D printing material would be strong enough to hold the sensor in position. The sensor holder was design to slide in between the existing bracket mount located on the ATV. This would provide a stable and fixed location for the sensor to operate successfully.

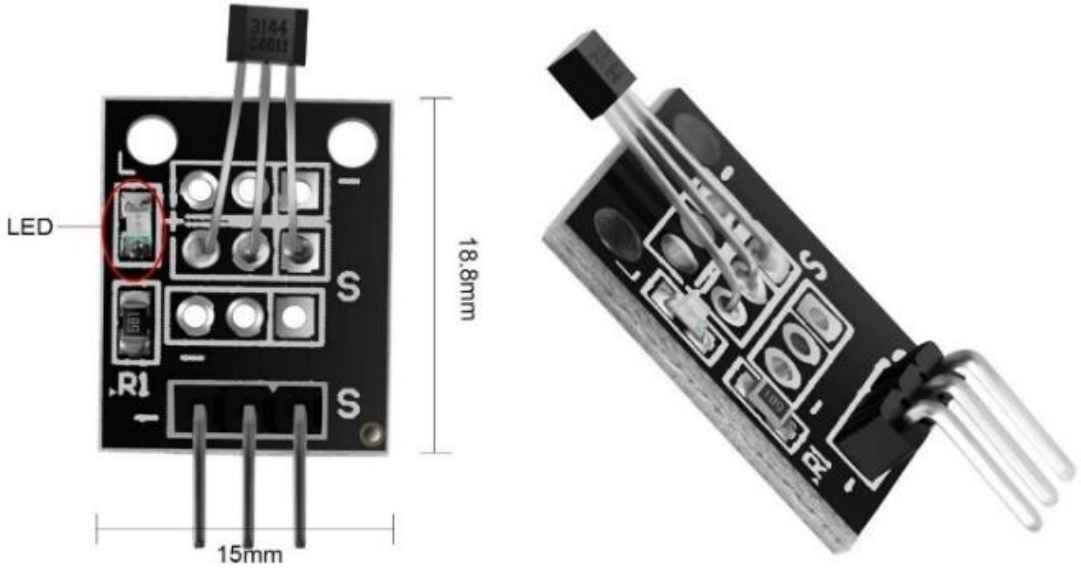

FIGURE 4.1: Hall Effect Sensor

After determining the dimensions of the ATV location space, the bracket was designed and printed. The design did not require any special CAD rendering so a straightforward design program like TINKERCAD was sufficient for developing a model. The model can be seen below in Figure 4.2. The dimensions shown are in millimeters.

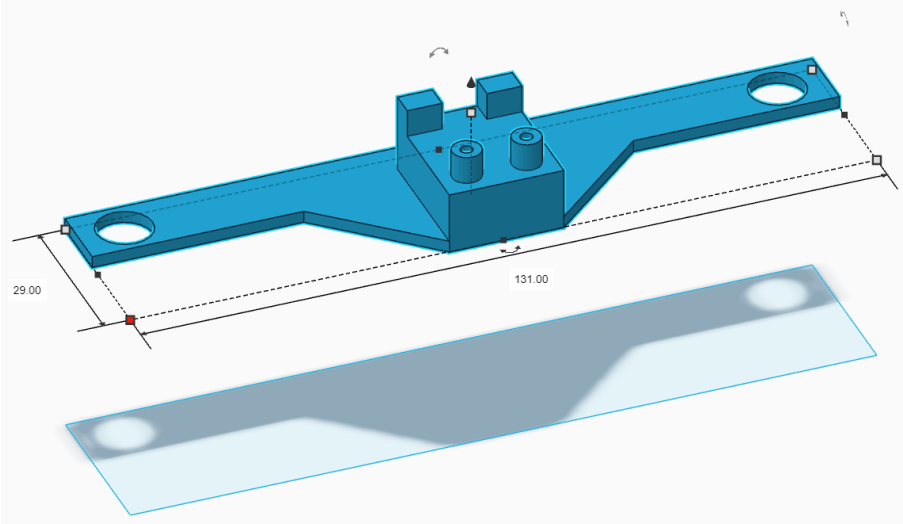

FIGURE 4.2: CAD model design of Hall effect sensor bracket

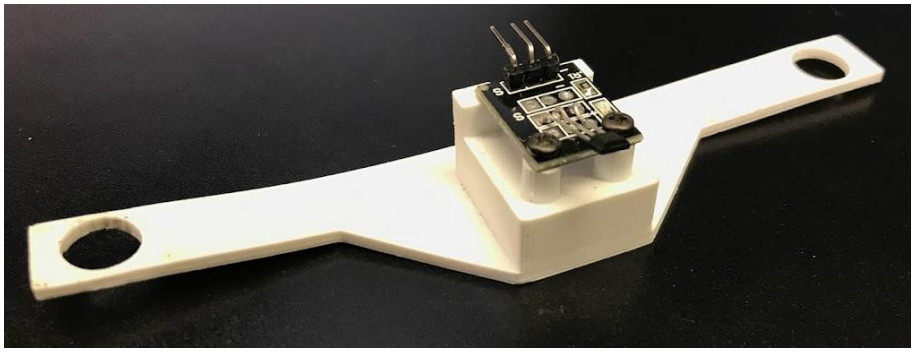

FIGURE 4.3: Completed Design

FIGURE 4.4: Sensor bracket installation

4.2 ENCODER DESIGN

The encoder design is based off a rotary shaft encoder. This type of encoder is attached to the shaft or axle as it spins. There are magnets attached to the encoder that pass over a Hall effect sensor creating an electrical signal. The design specifications would need to allow the encoder to fit over and around the axle of the ATV and be able to attach magnets to the outer circumference. The magnets on the outer shell are representative of fractional distances of the circumference of the wheel. In Figure 4.5 below one can see how the wheel is evenly divided into sections. The starting point of each section completes a distance the wheel has travelled. The number of magnets on the encoder would be known as the encoder resolution. The more magnets there are the better the resolution of the encoder. This really makes a difference depending on the size of the wheel. The circumference of the ATV wheel is large at 1.93 meters. This means the size and number of magnets needed played a significant role in achieving an elevated level of discrete encoder resolution. The magnets must be small enough and spaced far enough apart so the Hall effect sensor can register when a new rising edge or pulse is detected. If the magnets are too close together the Hall effect sensor will always register a magnetic field present and signal a continuous high pulse.

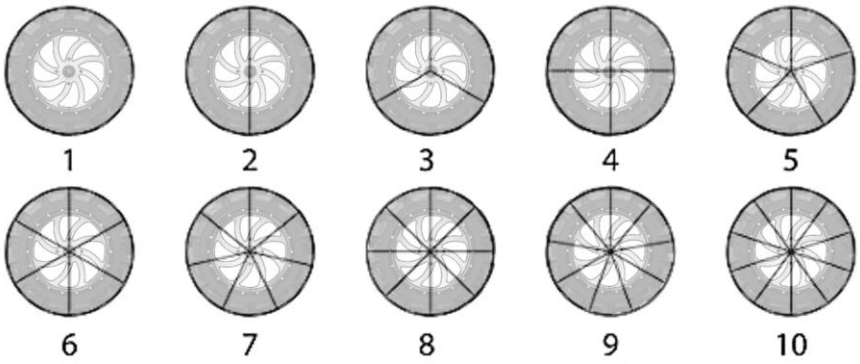

FIGURE 4.5: Encoder fractional distances of the ATV wheel

All the encoders were 3-D printed. The first encoder designed only held two magnets. The magnets were large at 25mm. The resolution for this size magnet was not sufficient. Another encoder was created that held three of the same magnets. This resolution was much better but still not good enough. Copies of the two encoders were printed and joined together to increase the resolution. The two-magnet encoder was increased to four, and the three-magnet encoder was increased to six. Combining the encoders to get a better resolution worked, but it increased the error because the magnets were too close together. Some of the pulses registered as one pulse decreasing the accuracy. A smaller size magnet was tried to get a better encoder resolution. A four-magnet encoder was designed to hold 12mm magnets. This did increase the resolution and worked well, but one more final encoder was created to hold eight of the 12mm magnets. This produced a resolution that was accurate enough to move on to testing.

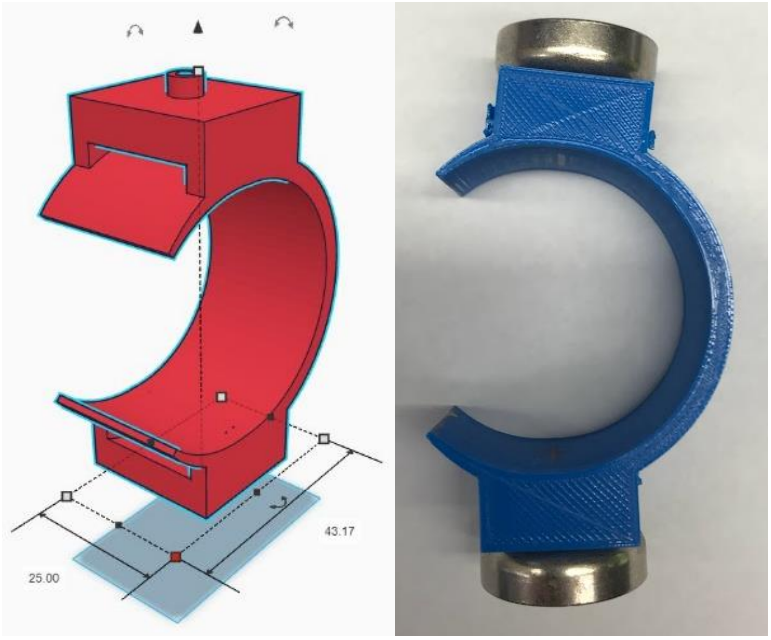

FIGURE 4.6: Encoder Design 1 (E1)

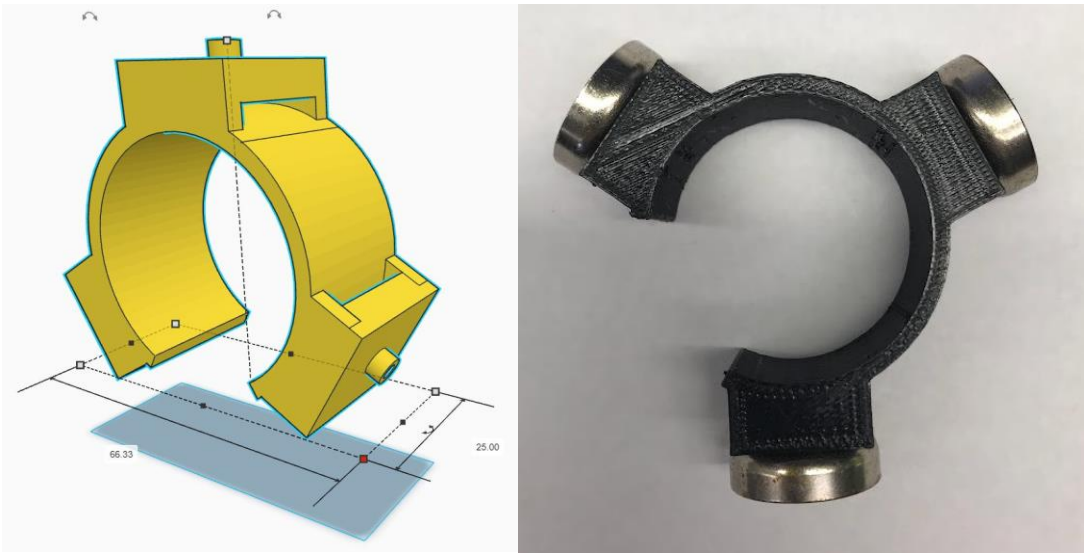

FIGURE 4.7: Encoder Design 2 (E2)

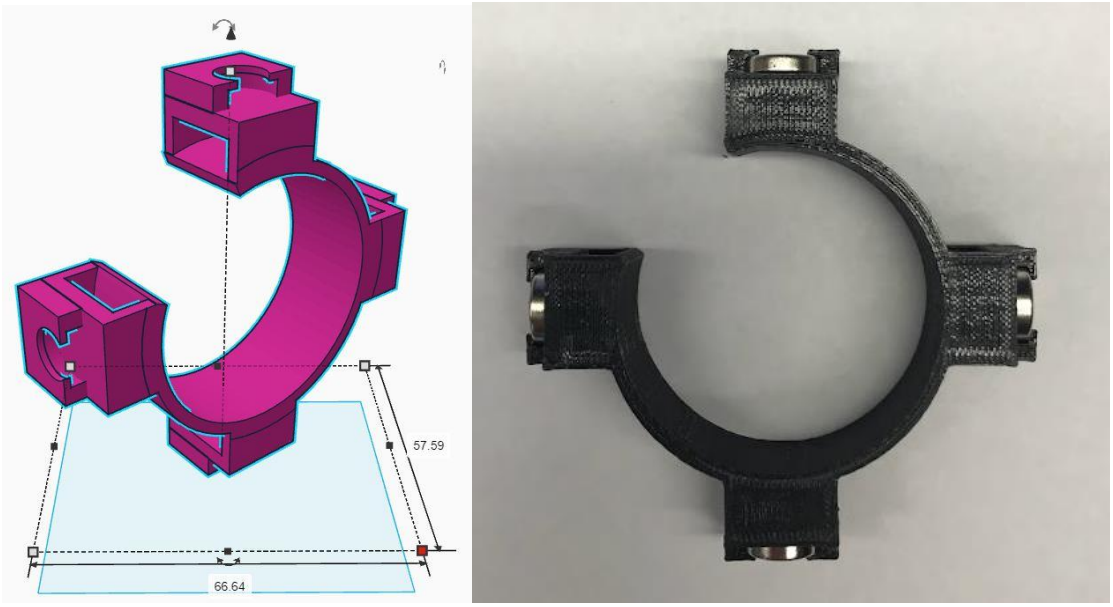

FIGURE 4.8: Encoder Design 5 (E5)

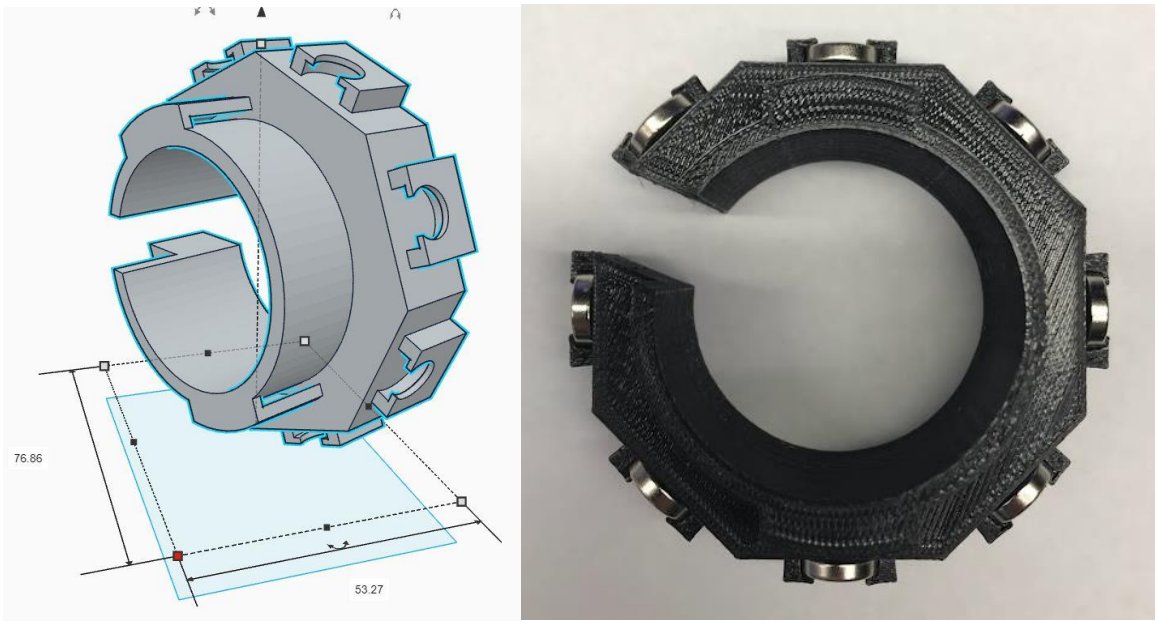

FIGURE 4.9: Encoder Design 6 (E6)

When mounting the encoders, the encoder needed to pass directly over the Hall effect sensor. This required there be enough space between the encoder and Hall effect sensor, so they do not hit each other and cause damage. Each encoder was designed to accept an adjustable stainless steel hose clamp. To mount the encoder the clamp would be adjusted until it was tight, and the encoder could not spin about the axle of the ATV. The distance between the Hall effect sensor and the magnet would be the last design parameter to check. The encoder design was able to be fully implemented and live testing began.

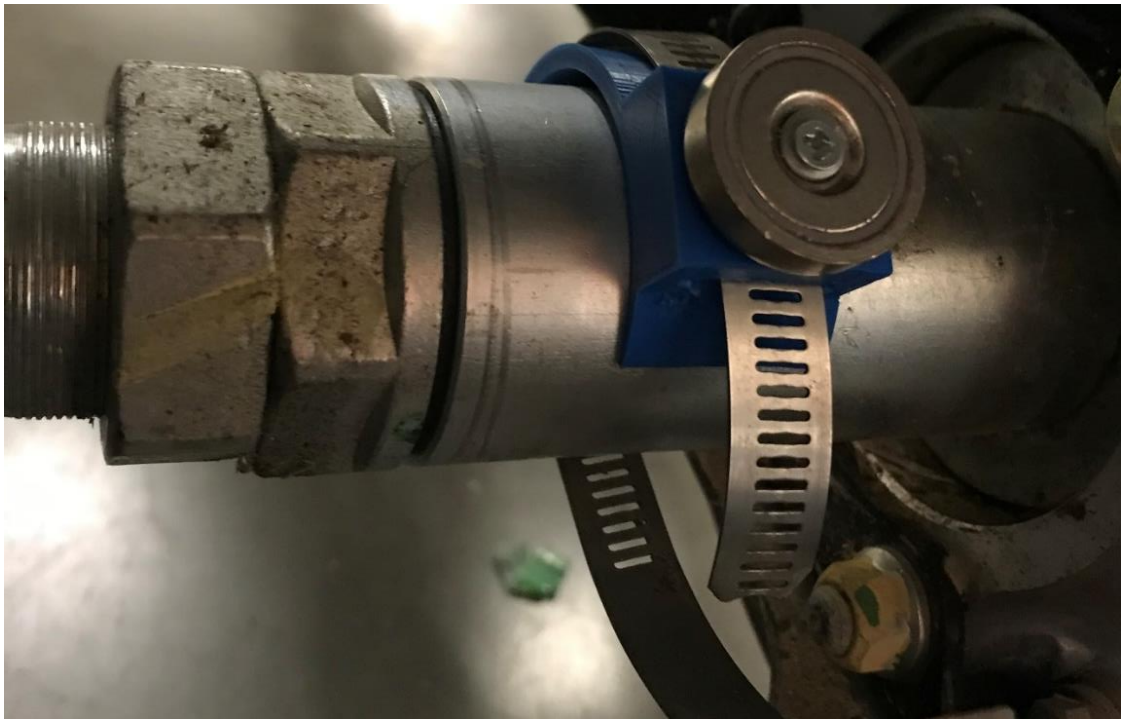

FIGURE 4.10: Installing encoder with adjustable clamp to the ATV axle

4.3 ENCODER LAB TESTING

Encoder testing began with manul checking of the sensors. The expected result when the magnet passed over the Hall effect sensor is a red light would switch on signifying the presence of the magnetic field. This was manually done with the ATV igntiion off and in neutral postion. This would allow someone to push the ATV slowly to see if the encoder rotation worked correctly. It was also important to make sure there was enough clearance between the encoder and the Hall effect sensor. If there was not enough clearance they would make contact and damage would occur. If there was to much clearance the magnet may not be close enough for the Hall effect sensor to detect the magnetic field. All of the parameters met and can seen in Figure 4.11 and Figure 4.12 below.

FIGURE 4.11: Distance clearance of encoder and Hall effect sensor

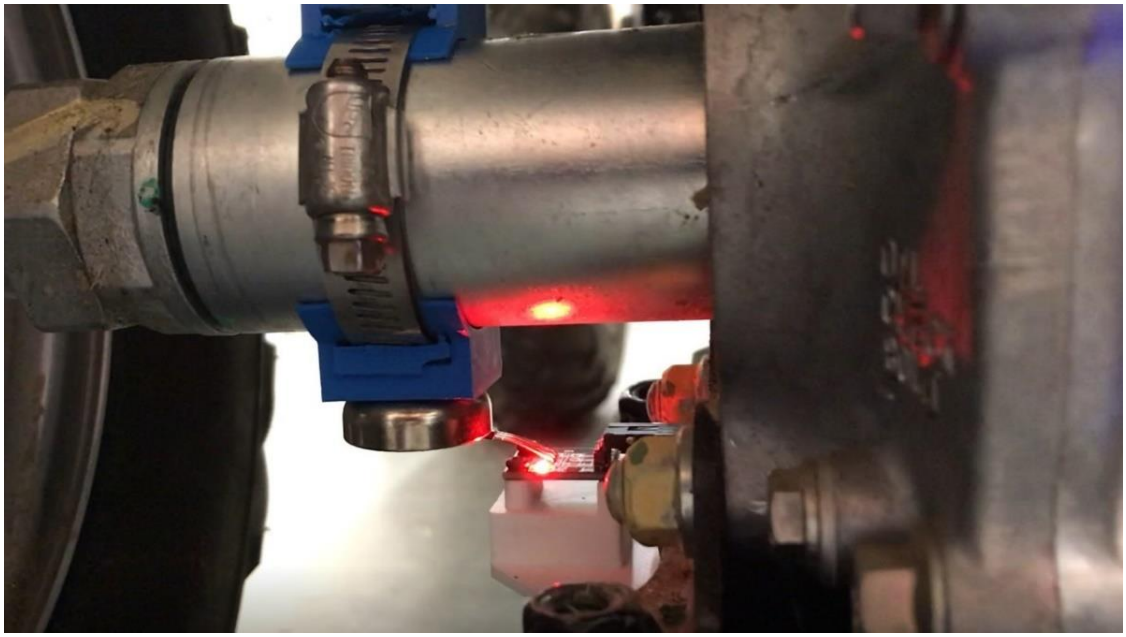

FIGURE 4.12: Hall effect sensor activation of magnetic field

The encoders were evaluated with MSP432 microcontrollers. This microcontroller provided the 5V DC supply needed to power the Hall effect sensor, and an interrupt service routine (ISR) needed to track the encoder pulses. A short algorithm was designed and coded with an ISR to track how many pulses were detected as the wheel of the ATV rotated. Measuring the size of the wheel and knowing how many magnets are on the encoder, we can determine how many pulses are expected per wheel rotation. For final testing, the eight-magnet encoder was used due to the finer resolution it produced.

$$diameter\ of\ wheel = d_w = 0.6143\ meters$$

$$Circumference\ of\ wheel = C_w = \pi d_w = \ 1.93\ meters$$

If the encoder has eight magnets, it is expected for eight pulses per wheel rotation,

$$Encoder\ Resolution = \frac{1.93}{8} = 0.2415\ meters\ per\ step \tag{3}$$

Distance travelled was calculated by the recurring summation of the number of pulses detected in one test session. A reset button was established on the microcontroller if this variable needed to be reset during the testing. The button would set the distance travelled variable back to zero. Integration over time of the distanced travelled was used to calculate velocity in meters per second shown in equation 4 below.

$$Velocity = \frac{distance\ (m)}{time\ (s)} = meters\ per\ second\ (MPS) \tag{4}$$

$$Speed = \frac{Velocity}{2.23694} = miles\ per\ hour\ (MPH) \tag{5}$$

As mentioned previously, there were errors encountered with the second and third encoders. The first two encoders worked but did not achieve the resolution needed. The first and second encoders were printed again, and the plan was to put two of the same encoders together to double the resolution. But, during testing it was found that the magnets were too large. This produced pulse errors for the Hall effect sensor because there was not enough distance between the presence of the magnetic field, generating one continuous pulse. This led to the final and sixth encoder design which produced a sufficient distance resolution.

TABLE 4.1: Initial encoder resolution and error

	Magnet Size (mm)	Number of Magnets (ppr)	Wheel Circumference (m)	Resolution (m)	Pulse Error
Encoder 1 (E1)	25	2	1.93	0.965	No
Encoder 2 (E2)	25	3	1.93	0.643	No
Encoder 3 (2xE1)	25	4	1.93	0.483	Yes
Encoder 4 (2xE2)	25	6	1.93	0.322	Yes
Encoder 5 (E5)	12	4	1.93	0.483	No
Encoder 6 (E6)	12	8	1.93	0.241	No

4.4 PREPARATION FOR FIELD TESTING

During testing it was extremely hard to check or monitor the speed or distance data from a computer terminal or serial monitor. The text was too small for most to see. Therefore, to monitor the speed output and the distance travelled data a GUI application was created to present the odometry of the encoder. This GUI was created using the application Qt Educational for students. The application was designed using the python coding language and a template modified for the project's needs. The GUI can be seen below in Figure 4.13. The odometer operated off serial communication from two MSP432 microcontrollers. One

com port tracked the distance travelled in meters and the speed in two different units (MPH and MPS). The second com port received the angle of the servo rotation that operated the throttle. This allowed the rider to monitor if the throttle was operating correctly during testing. This was a risk to the rider and the ATV if the servo did not disengage the throttle and could lead to wrecking the ATV or causing harm to spectators or the rider. To prevent this a remote relay was installed that could switch the ATV off in the case of an emergency.

FIGURE 4.13: Odometry GUI

The purpose of the application was to allow the rider to monitor the activity of the encoder and throttle while driving the ATV. To do this a Surface Pro tablet mount was designed, 3D printed, and attached in front of the steering wheel that allowed the rider to always view the application while driving. The design and mount can be seen in below in Figure 4.14.

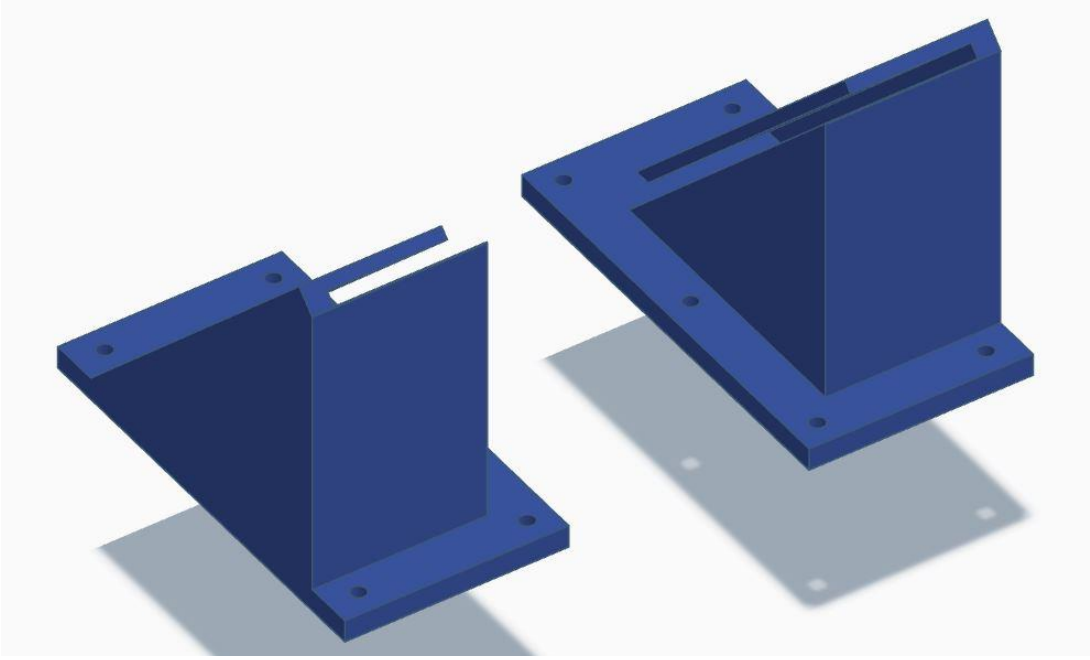

FIGURE 4.14: Laptop mount design

FIGURE 4.15: ATV laptop mount

A 3-D printed base station for the microcontrollers was installed on the rear of the ATV. The location of the base station needed to be close to the Hall effect sensor to minimize electrical interference during operation. The design enables the use of ten microcontrollers with stacking, and five without stacking. It was designed to hold the Texas Instruments (TI) MSP432, MSP430, and the TivaC microcontrollers. The base station can be seen in Figure 4.16 below.

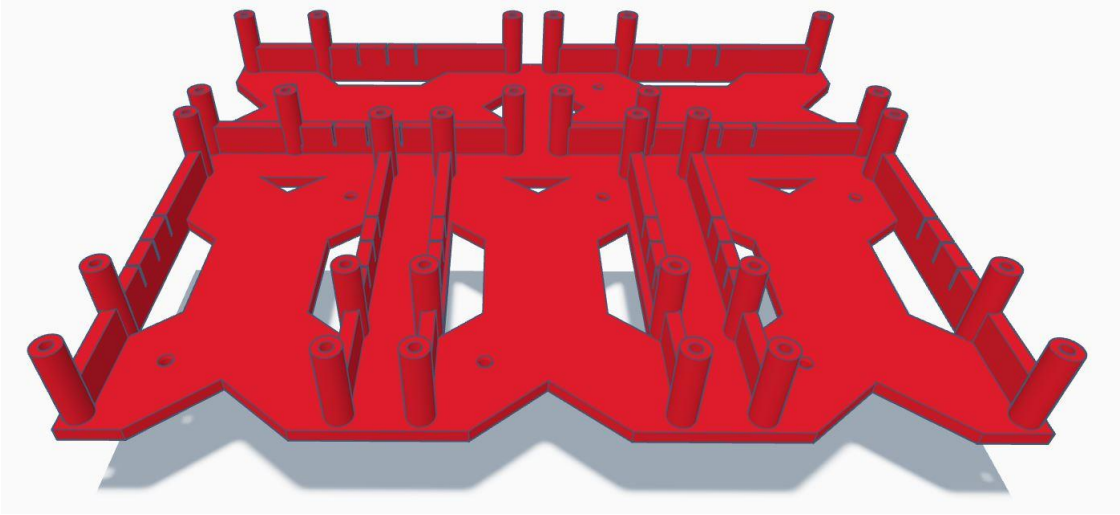

FIGURE 4.16: Microcontroller base station design

FIGURE 4.17: Microcontroller base station mount

4.5 ENCODER FIELD TESTING

Once all the tools and preparation were complete, actual field testing could begin. The purpose of this field testing was to investigate encoder and accuracy for longer distances. The location of testing was in the University of North Carolina at Charlotte garage yard, the side street to the university parking garage, and the Greenway path behind the school. The yard would be used for evaluating the ATV at short distances and slow speeds. The greenway path and side street would be used for longer distances and faster speeds.

For the yard testing a 30-meter straight line was measured and used for slow peed distance testing. The rider would start from point A and end at point B. The starting points are designated by the orange cones in Figure 4.18 below. The live results were displayed on the odometry application for the rider to see. During this test, the results showed that the distance travelled was much greater than the actual measured value by more than 10 percent. This issue was later resolved by changing the wheel circumference variable within the code. The new wheel circumference and encoder resolution can be seen in Table 4.2 below. The wheel was not inflated completely resulting in a new circumference measurement. After changing this variable, the data was accurate, and the path planned and the odometry results can be seen below. The distance measured by the encoder was 30.07 meters. This means the measured number of pulses was 138.

TABLE 4.2: New wheel circumference and resolution

	Magnet Size (mm)	Number of Magnets (ppr)	Wheel Circumference (m)	Resolution (m)	Pulse Error
Encoder 6 (E6)	12	8	1.743	0.2179	No

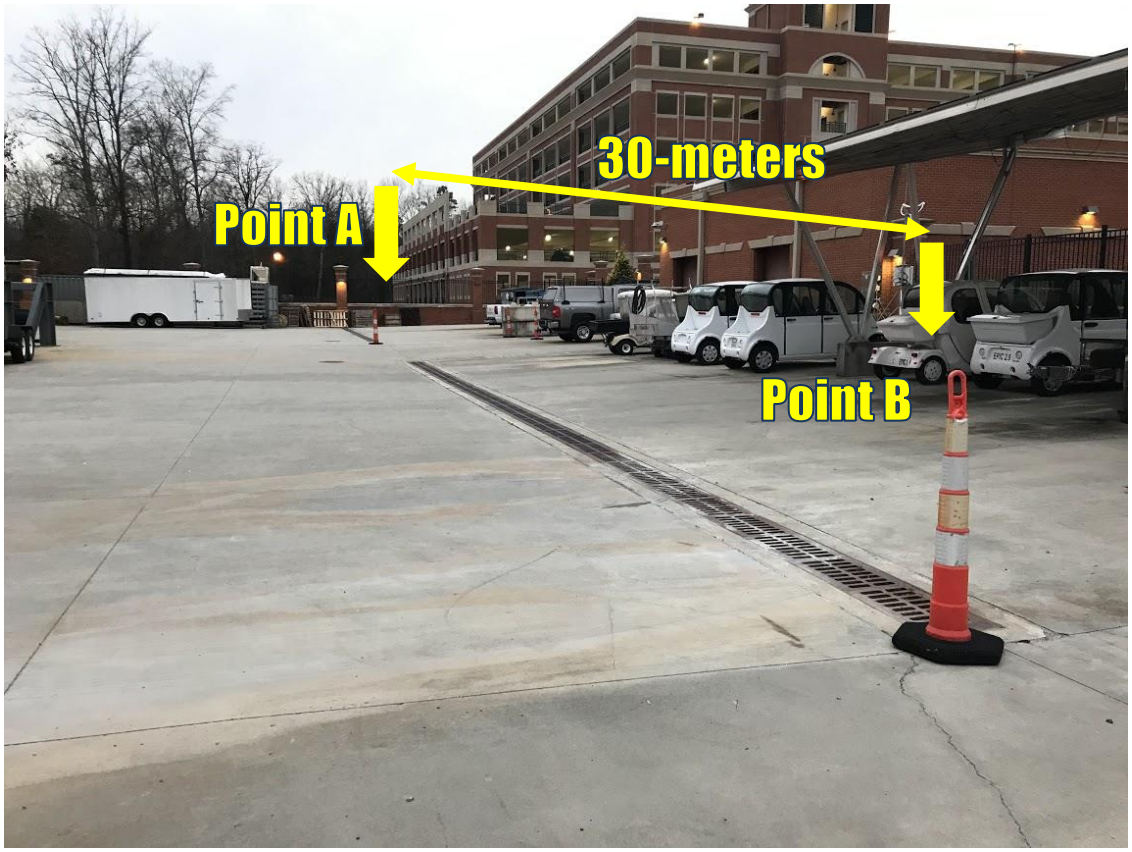

FIGURE 4.18: Straight 30-meter marked pathway in the yard

FIGURE 4.19: Odometry results from 30-meter measured drive

Google maps was used to plan the measured distances of the other pathways. There is a distance function within Google maps that allows “point to point” distance measuring.

Below are the mapped-out pathways for the greenway path and side street testing. The original point to point map on the left reported a rounded distance measurement 0.4 miles for the greenway path. The points had to be fined tuned to get a precision measurement of 0.346 miles seen in the map on the right. After traveling the mapped distance of the greenway the results were shown on the odometry display for the rider. The travelled distanced recorded by the encoder was 545.6 meters and can be seen in the Figure 4.21 below.

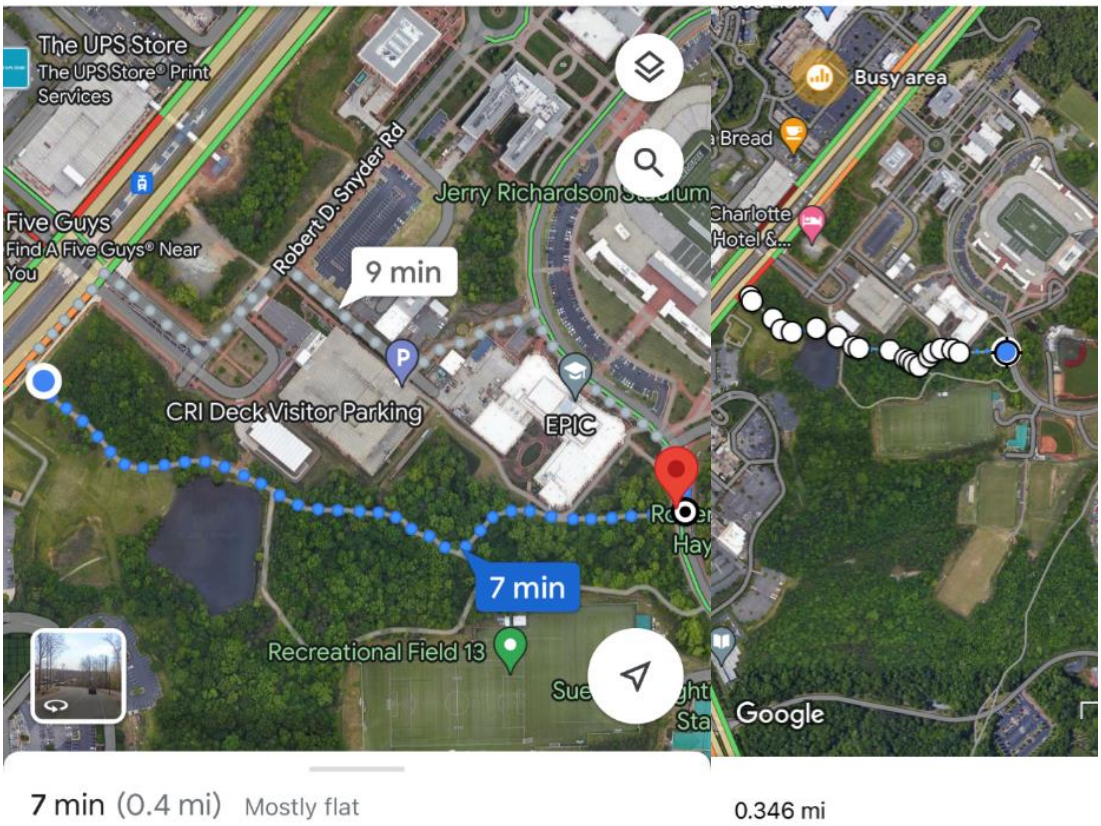

FIGURE 4.20: Greenway path mapping and total distance

FIGURE 4.21: Recorded distance for the greenway path

The next path recorded was the side street of the university parking garage. The Google measured distance of the path was 403.543 feet seen in the figure below. This translated to 122. 999 meters in distance. After travelling the path, the recorded distance by the ATV encoder was 121.8 meters seen in Figure 4.22 below.

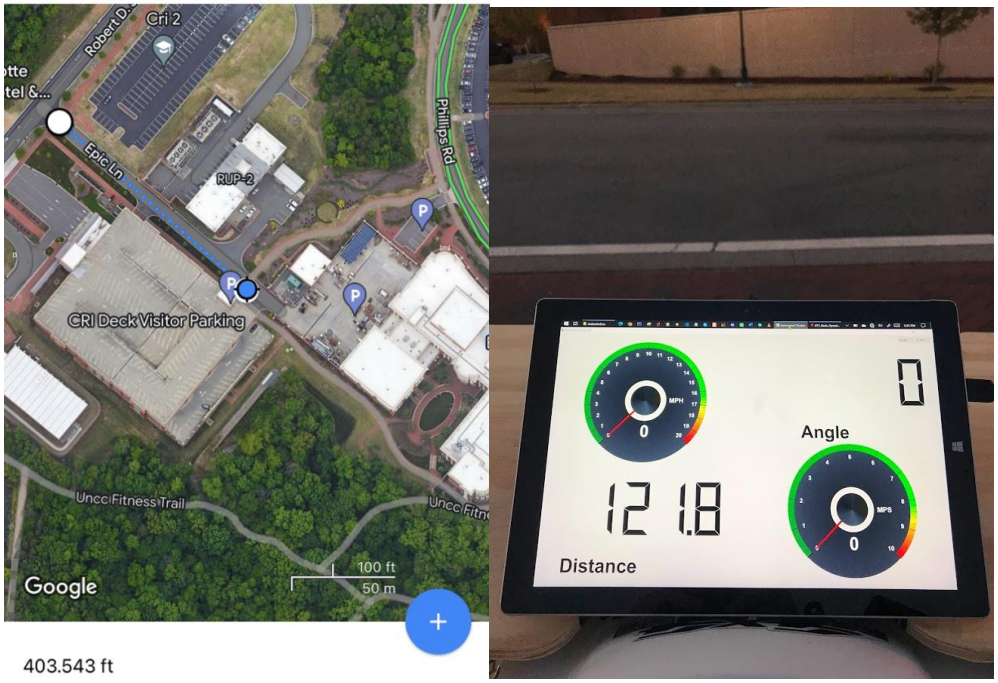

FIGURE 4.22: Mapped pathway and recorded encoder distance of side street

4.6 TEST RESULTS

The results of the encoder testing were sufficient to expectations. There was error expected in the results, but the error proved be to less than expected. The encoder worked better than expected in all criteria. There was speed tracking error involved. At slow to medium speed ranges of 0-19 MPH the speed was displayed on the odometer correctly. At speed ranges higher than 19 MPH the speed value seemed to be off by one value. This error was thought to be due to the engineering of the odometer of the ATV, but more testing would need to be done to make a final decision or provide a solution. The results of the encoder testing can be seen in the tables below.

TABLE 4.3: Results for encoder distance measurements

Path Measured	Expected (m)	Measured (m)	% Error
University Yard	30.00	30.07	+0.07
Greenway	556.83	545.60	-2.00
Side Street	122.99	121.80	-0.90

CHAPTER 5: CONCLUSIONS AND FUTURE WORK

5.1 CONCLUSIONS

Building the framework of an autonomous vehicle has proved to be challenging. There is a lot of testing and validation that goes into building the controls foundation of any vehicle or system. There will always be room for improvement. The successful implementation of the ATV encoder has opened the door to autonomy. Being able to get reliable feedback data about the ATV movement will allow the innovation of many more systems to be added. The throttle control for this application can now be fined tuned for velocity control. The encoder systems ease of use and the applications it can be used for makes doing further research feasible without questioning data validity about movement or velocity. This encoder application could be modified to work on many other vehicles easily.

5.2 FUTURE WORK

Future work on the ATV will include fine tuning the throttle operation. The throttle needs work on the coding algorithm for it to be able to handle increased or decreased slopes during travel. This tuning will autonomously allow it to speed up or slow down when hills are encountered in its path. The braking system will need to be re-installed to perform stopping and acceleration testing. The steering system that worked before will be modified to allow someone to ride the ATV while it is being controlled autonomously. A larger motor is planned to be installed to control the steering column directly. Eventually with the

tuning of the throttle, and the braking and steering systems working, more advanced autonomous algorithms will be tested with the ATV.

REFERENCES

[1] R. A. McKinney, M. J. Zapata, J. M. Conrad, T. W. Meiswinkel and S. Ahuja, "Components of an autonomous all-terrain vehicle," Proceedings of the IEEE SoutheastCon 2010 (SoutheastCon), 2010, pp. 416-419, doi: 10.1109/SECON.2010.5453838.

[2] A. Cortner, J. M. Conrad and N. A. BouSaba, "Autonomous all-terrain vehicle steering," 2012 Proceedings of IEEE Southeastcon, 2012, pp. 1-5, doi: 10.1109/SECon.2012.6196932.

[3] J. R. Henderson, J. M. Conrad and C. Pavlich, "Using a CAN bus for control of an All-terrain Vehicle," IEEE SOUTHEASTCON 2014, 2014, pp. 1-5, doi: 10.1109/SECON.2014.6950753.

[4] B. B. Rhoades and J. M. Conrad, "A Novel Terrain Topology Classification and Navigation for an Autonomous CAN Based All-Terrain Vehicle," SoutheastCon 2018, 2018, pp. 1-6, doi: 10.1109/SECON.2018.8479046.

[5] B. B. Rhoades, D. Srivastava and J. M. Conrad, "Design and Development of a ROS Enabled CAN Based All-Terrain Vehicle Platform," SoutheastCon 2018, 2018, pp. 1-6, doi: 10.1109/SECON.2018.8479285.

[6] K. H. Erian, S. Mhapankar, J. M. Conrad and S. Gambill, "System Integration over a CAN Bus for a Self-Controlled, Low-Cost Autonomous All-terrain Vehicle," 2019 SoutheastCon, 2019, pp. 1-8, doi: 10.1109/SoutheastCon42311.2019.9020379.

[7] K. H. Erian, J. M. Phillips and J. M. Conrad, "Design of a Control Architecture for an Autonomous All-Terrain Vehicle," 2021 IEEE 18th International Conference on Smart Communities: Improving Quality of Life Using ICT, IoT and AI (HONET), 2021, pp. 100-105, doi: 10.1109/HONET53078.2021.9615388.

[8] K. H. Erian and J. M. Conrad, "Controlling ATV Steering Angle on a Forest Path Using Machine Learning," SoutheastCon 2021, 2021, pp. 01-07, doi: 10.1109/SoutheastCon45413.2021.9401942.

[9] A. Babalola, R. Craven, S. Peddabavi and R. Belkacemi, "Real-time measurement of frequency using affordable rotary encoder and LabVIEW," IEEE SOUTHEASTCON 2014, 2014, pp. 1-6, doi: 10.1109/SECON.2014.6950647.

[10] B. Hou, Z. Tian, C. Li, Q. Wei, B. Zhou and R. Zhang, "A capacitive rotary encoder with a novel sensitive electrode," 2017 IEEE SENSORS, 2017, pp. 1-3, doi: 10.1109/ICSENS.2017.8234143.

[11] D. Rapos, C. Mechefske and M. Timusk, "Dynamic sensor calibration: A comparative study of a Hall effect sensor and an incremental encoder for measuring shaft rotational position," 2016 IEEE International Conference on Prognostics and Health Management (ICPHM), 2016, pp. 1-5, doi: 10.1109/ICPHM.2016.7542858.

[12] Ching-Chuan Su, "Mechanisms for the longitudinal recoil force in railguns based on the Lorentz force law," in IEEE Transactions on Magnetics, vol. 42, no. 9, pp. 2193-2195, Sept. 2006, doi: 10.1109/TMAG.2006.878010.

[13] “A3141, A3142, A3143, and A3144 - elecrow.com.” [Online]. Available: https://www.elecrow.com/download/A3141-2-3-4-Datasheet.pdf.

[14] K. Takaya, T. Asai, V. Kroumov and F. Smarandache, "Simulation environment for mobile robots testing using ROS and Gazebo," 2016 20th International Conference on System Theory, Control and Computing (ICSTCC), 2016, pp. 96-101, doi: 10.1109/ICSTCC.2016.7790647.

[15] “A3141, A3142, A3143, and A3144 - elecrow.com.” [Online]. Available: https://www.elecrow.com/download/A3141-2-3-4-Datasheet.pdf.

[16] A. F. Ilmiawan, D. Wijanarko, A. H. Arofat, H. Hindersyah and A. Purwadi, "An easy speed measurement for incremental rotary encoder using multi stage moving average method," 2014 International Conference on Electrical Engineering and Computer Science (ICEECS), 2014, pp. 363-368, doi: 10.1109/ICEECS.2014.7045279.

[17] J. Janisch, “Understanding Integrated Hall Effect Rotary encoders,” *Fierce Electronics*, 01-Nov-2006. [Online]. Available: https://www.fierceelectronics.com/components/understanding-integrated-hall-effect-rotary-encoders.

[18] D. Rapos, C. Mechefske and M. Timusk, "Dynamic sensor calibration: A comparative study of a Hall effect sensor and an incremental encoder for measuring shaft rotational position," 2016 IEEE International Conference on Prognostics and Health Management (ICPHM), 2016, pp. 1-5, doi: 10.1109/ICPHM.2016.7542858.